ACS APPLIED MATERIALS & INTERFACES

Research Article

www.acsami.org

Epoxidized Soybean Oil/ZnO Biocomposites for Soft Tissue Applications: Preparation and Characterization

Ana M. Díez-Pascual*,† and Angel L. Díez-Vicente‡

†Analytical Chemistry, Physical Chemistry and Chemical Engineering Department, Faculty of Biology, Environmental Sciences and Chemistry, Alcalá University, 28871 Alcalá de Henares, Madrid, Spain

‡Airbus Operations S. L., John Lennon s/n, 28906 Getafe, Madrid, Spain

ABSTRACT: Biocompatible and biodegradable nanocomposites comprising epoxidized soybean oil (ESO) as matrix, zinc oxide (ZnO) nanoparticles as reinforcements, and 4-dimethylaminopyridine (DMAP) as a catalyst have been successfully prepared via epoxidization of the double bonds of the vegetable oil, ultrasonication, and curing without the need for interfacial modifiers. Their morphology, water uptake, thermal, mechanical, barrier, tribological, and antibacterial properties have been investigated. FT-IR analysis revealed the existence of strong ESO−ZnO hydrogen-bonding interactions. The nanoparticles acted as mass transport barriers, hindering the diffusion of volatiles generated during the decomposition process and leading to higher thermal stability, and also reduced the water absorption and gas permeability of the bioresin. Significant improvements in the static and dynamic mechanical properties, such as storage and Young's moduli, tensile strength, toughness, hardness, glass transition, and heat distortion temperature, were attained on reinforcement. A small drop in the nanocomposite stiffness and strength was found after exposure to several cycles of steam sterilization or to simulated body fluid (SBF) at physiological temperature. Extraordinary reductions in the coefficient of friction and wear rate were detected under both dry and SBF conditions, confirming the potential of these nanoparticles for improving the tribological performance of ESO. The nanocomposites displayed antimicrobial action against human pathogen bacteria with and without UV illumination, which increased progressively with the ZnO content. These sustainable, ecofriendly, and low-cost biomaterials are very promising for use in biomedical applications, like structural tissue engineering scaffolds.

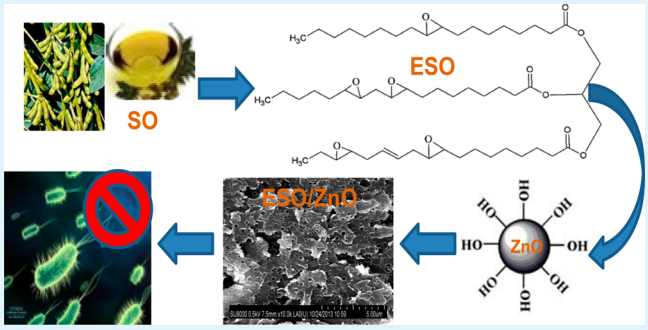

KEYWORDS: *epoxidized soybean oil, bionanocomposites, ZnO nanoparticles, antimicrobials, tissue engineering*

1. INTRODUCTION

Worldwide demand for biobased products derived from renewable biomass has increased dramatically over the past few years due to global environmental concerns and the sharp rise in petroleum price. In this context, cost-effective, sustainable, and ecofriendly polymeric materials derived from renewable resources that can replace those based on petroleum feedstock are being sought. The most employed renewable resources are plant oils, polysaccharides, and proteins. Vegetable oils are highly suitable starting materials for polymers due to their abundance, low cost, biodegradability, environmental benefits, and variety of functional groups.[1] They are triglycerides with varying composition of fatty acids depending on the plant, crop, season, growing conditions, and purification methods,[2] and their properties are conditioned by the stereochemistry of the double bonds, the degree of unsaturation, and the length of the fatty acids. Linseed, sunflower, castor, soybean, oiticica, palm, tall, and rapseed oils are the most commonly used for the synthesis of biopolymers.[3,4] Thermal or cationic polymerization of these vegetable oils with styrene or divinylbenzene can be performed to obtain thermosetting biomaterials, ranging from elastomers to rigid engineering polymers.[4,5] Recently, bionanocomposites derived from these vegetable-oil-based thermosets with improved properties have been developed.[6,7]

Soybean oil (SO) is available abundantly across the world, and is the second largest crop plant in the U.S. The unsaturated sites in SO can be used to introduce new functional groups like epoxides, and epoxidized soybean oil (ESO) is already available on the market. ESO can be used as a stabilizer and plasticizer in polymers or as an additive in lubricants and can also be converted into polyols by ring opening of the oxirane groups, resulting in intermediates that are used in polyurethane materials.[8] Its sustainability, low price, and ease of manufacture make this bioresin an attractive alternative to petroleum-based plastics. In this regard, it has already been employed as raw material for the synthesis of new polymers[9] as well as in paints and coatings,[10] and it is starting to be used in environmentally sensitive industries like agriculture, food packaging, and biomedicine. Thus, SO exhibits antimicrobial activity against

Received: August 11, 2014
Accepted: September 15, 2014
Published: September 15, 2014

Table 1. Fatty Acid Composition of Soybean Oil

soy fatty acid		structure		%
saturated	palmitic	$CH_3(CH_2)_{14}COOH$	C16:0	11
	stearic	$CH_3(CH_2)_{16}COOH$	C18:0	4
unsaturated	oleic	$CH_3(CH_2)_7CH{=}CH(CH_2)_7COOH$	C18:1	26
	linoleic	$CH_3(CH_2)_4CH{=}CH{-}CH_2{-}CH{=}CH(CH_2)_7COOH$	C18:2	52
	linolenic	$CH_3{-}CH_2{-}CH{=}CH{-}CH_2{-}CH{=}CH{-}CH_2{-}CH{=}CH(CH_2)_7COOH$	C18:3	7

food borne pathogens (i.e., *Escherichia coli*, *Pseudomonas aeruginosa*, *Staphylococcus aureus*, *Vibrio cholerae*, and *Salmonella enteritidis*),[11] and the bioactivity of soybean-based materials on cellular components of regenerating tissues has been recently demonstrated.[12] Moreover, Wong et al.[13] prepared anionic polymers from ESO and used them as carriers for anticancer drugs, and Miao et al.[14] synthesized polyurethane networks based on soybean oil as scaffolds. ESO can be metabolized in the human body and is biocompatible and biodegradable; hence, it presents a variety of biomedical applications ranging from surgical sealants and glues, stents, pharmacological patches, wound healing devices, and drug carriers to scaffolds for tissue engineering.[15,16] This field aims to restore, maintain, or improve tissue functions that are defective or have been lost by different pathological conditions, either by developing biological substitutes or by reconstructing tissues. Scaffolds play a key role in tissue regeneration and repair.[15] They are 3D biomaterials with an interconnected pore structure that ensures sufficient transport of gases and adequate diffusion of nutrients for cell growth and proliferation. They need to be biocompatible, biodegradable, and have good water and oxygen permeability. Further, to become clinically viable, they should be cost-effective and easy to scale up.

Thermosets are highly cross-linked polymers cured by heat, pressure, light radiation, or a combination of these energy sources. The double bonds present in the unsaturated fatty acids of the vegetable oils can be used as reaction sites for the cross-linking process, and the material properties are conditioned by the degree of cross-linking: those with a high cross-linking density display good mechanical and thermal properties.[17] There are four main routes to produce epoxides from olefinic molecules:[18,19] epoxidation with percarboxylic acids, the most used in industry; epoxidation with organic and inorganic peroxides; epoxidation with halohydrins, which is environmentally unfriendly since it uses hypohalous acids and their salts as reagents; and epoxidation with molecular oxygen, which is more "green" and economically viable when silver is used as a catalyst, although it leads to low levels of double bond conversion and may result in vegetable oil degradation. One of the most suitable and efficient techniques for epoxidation is the reaction with formic acid and hydrogen peroxide.[19]

Recently, zinc oxide (ZnO) nanostructures have attracted much attention as future materials due to their low cost, easy availability, the possibility of performing surface modifications with different functional groups, and biocompatibility. With a wide band gap of 3.4 eV and a large exciton binding energy of 60 meV at room temperature, they are widely used for optical devices.[20] These environmentally friendly materials possess a large volume to area ratio; crystalline structure; radiation hardness; good mechanical properties, including a Young's modulus of 111 GPa and hardness of ∼5 GPa;[20] low coefficient of thermal expansion (∼2.5 × 10^{-6} K^{-1} at 300 K); and high thermal conductivity (∼1 W cm^{-1} K^{-1})[21] and hence are highly suitable as catalysts, gas sensors, or reinforcing fillers in polymer composites.[22−24] They also display antimicrobial activity in the pH range of 7−8, even in the absence of light,[25] and have been extensively employed as antimicrobials against both Gram-positive and Gram-negative bacteria; further, they are considered to be nontoxic, and recent studies have demonstrated that they are not harmful to the DNA of human cells.[26]

Triglyceride-based materials exhibit low rigidity and strength, which limit their use for practical applications.[27] Several attempts have been made to improve the thermal and mechanical properties of ESO polymers by reinforcing with natural fibers,[28] silica,[29] or nanoclay.[30] The present study focuses on the development and characterization of bionanocomposites from ESO and ZnO nanoparticles. The composite performance is strongly affected by the dispersion of the nanofillers and their interfacial interactions with the matrix. The effect of reinforcement on properties, such as mechanical, thermal, tribological, barrier, and antibacterial, are investigated in detail. These novel biomaterials with antimicrobial function show great potential for biomedical applications, particularly as scaffolds for soft tissue engineering.

2. EXPERIMENTAL SECTION

Materials. SO was supplied by CEVAL and used without purification. Its major properties are iodine value = 137, oxidation level (PV) = 0.9, acid value = 0.8, $d_{25°C}$ = 0.92 g/cm^3, and M_w ∼ 868 g/mol, and it contains ∼4.7 double bonds per triglyceride molecule. Its fatty acid composition is given in Table 1. ZnO nanopowder, <100 nm particle size and specific surface area in the range of 15−25 m^2/g, and 4-dimethylaminopyridine (DMAP), $C_7H_{10}N_2$, were supplied by Sigma-Aldrich. Formic acid (98%) and hydrogen peroxide (33%) were provided by Panreac Química S.L.U.

Epoxidation Reaction. First, SO and formic acid were added to a four-necked reaction vessel equipped with a mechanical stirrer and thermometer and mixed for 10 min at 700 rpm and 50 °C. To start the epoxidation, H_2O_2 was added dropwise to the mixture for 1 h. 1:1.7 mol ratios of carbon double bonds to H_2O_2 were used. The reaction was allowed to proceed for 5 h at 50 °C. Subsequently, the mixture was cooled down and washed with water three times (cool, hot, cool) to eliminate the residual acid and then filtered. To remove any remaining water, the resin was further dried with anhydrous sodium sulfate in an oven at 70 °C for 12 h. The synthesis procedure of ESO is shown in Scheme 1. The FT-IR spectra (Figure 1) confirmed the success of the epoxidation reaction. The oxirane content (6.3%) was determined by titration of the epoxy groups with hydrobromic acid solution in glacial acetic acid.[31]

Preparation of the Nanocomposites. ESO was mixed with DMAP catalyst (3.0 wt %) at 100 °C for 5 min using a mechanical stirrer. The mixture was degassed, poured into silicone molds, and cured in a vacuum oven at 120 °C overnight. An analogous procedure was used to prepare ESO-based nanocomposites containing 1.0, 3.0, 5.0, and 7.0 wt % ZnO. The nanoparticles were homogeneously dispersed in ESO at 100 °C using an ultrasonicator for 30 min, and subsequently DMAP was added, followed by curing under the aforementioned conditions.

Characterization Techniques. The morphology of the nanocomposites was examined with a SU8000 Hitachi scanning electron microscope (SEM). Samples were cryofractured in liquid nitrogen and

Scheme 1. Synthesis Procedure of Epoxidized Soybean Oil (ESO)

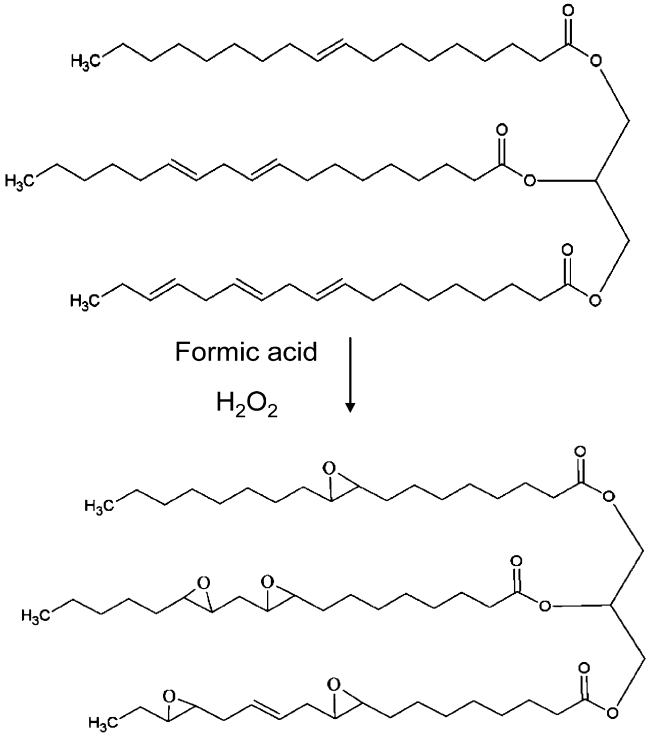

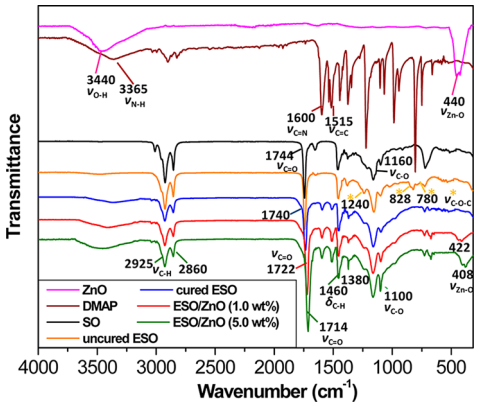

Figure 1. FT-IR spectra of ZnO, SO, DMAP, ESO (both cured and uncured), and the nanocomposites with 1.0 and 5.0 wt % nanoparticle content.

then coated with a ∼5 nm Cr overlayer to avoid charge accumulation during electron irradiation.

The attenuated total reflectance FT-IR spectra were acquired at 25 °C on a PerkinElmer Spectrum One spectrometer equipped with a Universal ATR sampling accessory (diamond crystal) and a red laser excitation source (632.8 nm). Spectra were recorded in the range between 4000 and 400 cm^{-1}, with an incident laser power of 1 mW and resolution of 4 cm^{-1}.

The thermal stability of the composites was analyzed by TGA using a TA Instruments Q50 thermobalance at a heating rate of 10 °C/min. The temperature was scanned from room temperature to 550 °C under a nitrogen atmosphere, with a purge gas flow rate of 60 mL/min.

To determine the water absorption, samples were dried in a desiccator at 0% RH for 1 week. Subsequently, they were placed in a beaker at 100% RH and allowed to absorb water at 25 ± 2 °C. Every 48 h, the samples were taken out, the water on their surface was removed, and samples were weighed and immediately replaced into the water. Water uptake was calculated as $[(W_t - W_i)/W_i] \times 100$, where W_i and W_t are the initial and instantaneous weight, respectively. Five replicates for each nanocomposite were measured.

Water vapor permeability (WVP) was determined at 25 °C following the ASTM E96-95 standard using Payne permeability cups of 3.5 cm diameter. Samples were equilibrated at 54% RH using magnesium nitrate-6-hydrate. WVP was calculated as WVP = $(\Delta ml)/(At\Delta P)$, where Δm is the weight loss of each cup, l the thickness of the film, A the contact area, t the time, and ΔP the partial pressure difference between the inside and outside of the cup. Tests were replicated four times, and average values are reported.

Oxygen permeability (O_2P) was evaluated at 25 °C on films equilibrated at 54% RH by measuring the oxygen transference rate (OTR) with a gas permeability tester (Ox-Tran 1/50 System), following the ASTM D3985-05 standard. O_2P was calculated following the expression $O_2P = (OTR \times l)/\Delta P$, where l is the film thickness and ΔP the difference between oxygen partial pressures across the film. The results were taken as the average of three tests.

The dynamic mechanical performance was studied using a Mettler DMA861 dynamic mechanical analyzer. Measurements were carried out in the tensile mode on rectangular bars, in the range between −125 and 100 °C, at a heating rate of 2 °C/min and frequency of 1 Hz.

Tensile properties were measured with an INSTRON 4204 mechanical tester at 23 ± 2 °C and 50 ± 5% RH, using a crosshead speed of 1 mm/min, according to the UNE-EN ISO 527-1 standard. Five specimens for each type of nanocomposite were measured. Tensile tests were also performed on composites subjected to 10 steam sterilization cycles in an autoclave in which they were exposed to saturated steam for 15 min at 124 °C and 2 bar, following the UNE-EN ISO 17665 standard, as well as on samples soaked in a simulated body fluid (SBF) at 37 °C for 10 weeks. The electrolyte used as SBF was Hank's balanced salt solution (HBSS).[32]

Charpy notched impact strength tests were carried out on a CEAST Fractovis dart impact tester, according to the ASTM D 6110-10 standard. Measurements were performed at 23 ± 2 °C and 50 ± 5% RH. The data correspond to the average value of seven specimens.

The heat distortion temperature (HDT) was measured using a HDT/VICAT heat deflection tester according to the ASTM D648 standard. Specimens were conditioned at 25 ± 2 °C and 50 ± 5% RH for 24 h prior to the measurements. The sample position was edgewise, with test span 100 mm, surface stress 1.8 MPa, and heating rate 2 °C/min.

The coefficient of thermal expansion (CTE) was measured by thermomechanical analysis (TMA) using a PerkinElmer TMA 7 device. Samples were heated from 0 to 250 °C at 2 °C/min, and the CTE was determined from the slope of the TMA curve both above and below T_g.

A micro-Vickers hardness tester (Innovatest 422A) was used to evaluate the microhardness. Specimens were subjected to a load of 50 g for 15 s under controlled conditions. The diagonals of each indentation were measured three times to obtain average values.

Pin-on-disk tests were carried out on a pin-on-disk tribometer (MT/10/SCM from Microtest) at a speed of 375 rpm using a 6 mm diameter 100Cr6 steel ball. The equipment was placed in an isolated box, and the experiments were performed under both dry and lubricated (SBF) conditions over 6 h. For the dry tests, a load of 5 N was applied at 23 ± 2 °C and 10 ± 2% RH. Experiments in SBF medium were performed at 37 °C under 10 N load, using a sample tray holder coupled directly to the tribometer plate. The wear experienced by the substrate was determined by measuring the wear-track profile with a profilometer. Each test was repeated three times.

The antibacterial activity assay was performed following the ISO 22196:2007 standard. The composites were tested against Gram-positive *S. aureus* (ATCC 12600) and Gram-negative *E. coli* (ATCC 25922) bacteria. The samples were sterilized in an autoclave prior to the tests and then submerged in a 3-day-old nutrient broth of ∼2.0 × 10^6 colony forming units per mL (cfu/mL). After incubation at 37 °C for 24 h, the number of cfu per sample was counted manually. In one set of experiments, the samples were illuminated with 365 nm UV

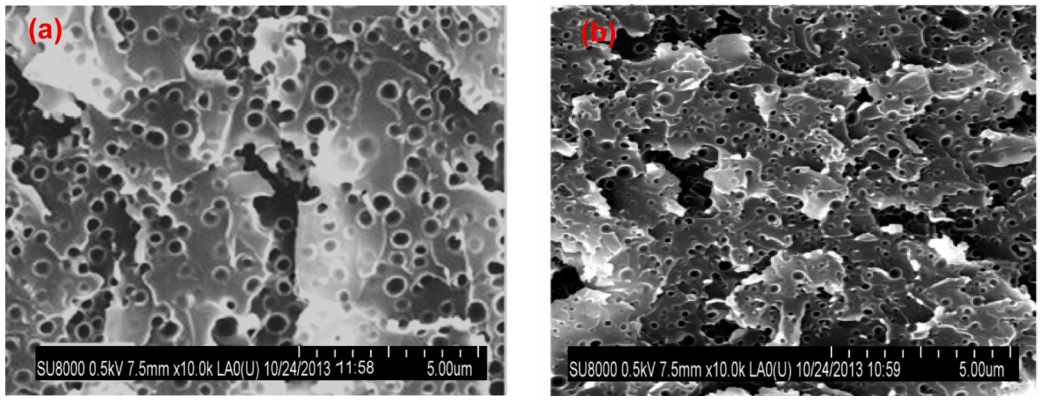

Figure 2. SEM micrographs of ESO (a) and ESO/ZnO (5.0 wt %) nanocomposite (b).

light, and in the other set they were tested without UV irradiation. The antibacterial activity was calculated as log[(viable cell count$_{control}$)/(viable cell count$_{composite}$)], where a flask containing bacteria and no sample was used as control. The tests were conducted in triplicate.

3. RESULTS AND DISCUSSION

FT-IR Study. The ATR-FTIR spectra of SO, ESO (both uncured and cured), DMAP, ZnO, and the nanocomposites with 1.0 and 5.0 wt % loading are compared in Figure 1 to confirm the epoxidation reaction and give insight into the nanoparticle−matrix interactions. The spectrum of ZnO displays a broad and intense peak centered at about 3440 cm^{-1} assigned to the stretching of surface-absorbed water and hydroxyl groups on the nanoparticle surface and an intense peak at 440 cm^{-1} that corresponds to the stretching of Zn−O bonds.[22] SO presents intense signals at 1744 and 1160 cm^{-1} related to the C═O and C−O stretching, respectively, in triglyceride molecules.[33] The peaks at 2925 and 2860 cm^{-1} arise from the asymmetric and symmetric C−H stretching in methylene groups, while their asymmetric and symmetric bending appear at 1460 and 1380 cm^{-1}, respectively, and the bands at 3020, 1650, and 720 cm^{-1} respectively correspond to stretching vibrations of double bonds: ═C−H, C═C, and *cis*-CH═CH.[33] New signals can be observed in the spectrum of uncured ESO at 1240, 828, and 780 cm^{-1} referred to different C−O−C stretching modes of the oxirane ring,[34] together with the disappearance of the bands at 3020 and 1650 cm^{-1}, thus corroborating the success of the epoxidation reaction. The bands related to the epoxy group are hardly visible in the spectrum of the cured ESO, simultaneous with the increase of the intensity of a band at ∼1100 cm^{-1} related to the C−O stretching of the ether group that overlaps with the C−O vibration of the triglicerides. Besides, some bands arising from DMAP catalyst are detected: the N−H stretching in the range of 3580−3150 cm^{-1} overlapping with the O−H stretching of hydroperoxide groups formed through oxirane ring opening, C═N and C═C stretching bands between 1600 and 1515 cm^{-1}, and out-of-plane C−H bending bands between 690 and 600 cm^{-1}.[34]

The spectra of the nanocomposites show the characteristic peaks of both cured ESO and ZnO. A broadening and upshift of the peak assigned to the O−H and N−H stretching is observed, by ∼40 and 75 cm^{-1} for the composites with 1.0 and 5.0 wt % ZnO, respectively. Such behavior has been attributed to a change from intramolecular to intermolecular H-bonding interactions[35] and suggests H-bond formation with the carbonyl of the ester group of ESO at the expense of breaking the H-bonds among hydroxyl groups of the nanoparticles. Besides, the C═O stretching in the nanocomposites is wider and shifted to lower wavenumber compared to that of cured ESO, the downshift being ∼18 and 26 cm^{-1} at 1.0 and 5.0 wt % loading, yet another indication of the formation of hydrogen bonds with the hydroxyl moieties of the nanoparticles. The Zn−O stretching band also shifts down to 422 and 408 cm^{-1} in the nanocomposites with 1.0 and 5.0 wt %, respectively, corroborating the existence of nanoparticle−matrix interactions that become stronger with increasing nanofiller concentration.

SEM Analysis. The cured bioresin and the nanocomposites were found to be transparent and flexible. Their cryofractured surface was analyzed by SEM, and representative micrographs of ESO and ESO/ZnO (5.0 wt %) are shown in Figure 2. The image of ESO reveals a porous morphology, with numerous spherical pores (about 300 nm size). However, in the nanocomposite the pore size significantly decreases, by ∼50%, and the surface roughness increases, which could be indicative of a more tortuous crack propagation path. The nanoparticles, with quasi-spherical shape and a mean diameter of 80 nm, appear as bright dots in the images and are randomly and very well dispersed. A similar morphology with uniformly dispersed nanofillers was also found for the rest of nanocomposites, demonstrating that the interactions between the polar groups of the matrix and the hydroxyl groups of the ZnO prevent nanoparticle aggregation. The images confirm the successful dispersion of the nanoparticles without the need for particle surface treatments or compatibilizers, making the processing of these biomaterials simple, economic, and environmentally friendly.

Thermal Stability. The thermal stability of ESO-based bionanocomposites was evaluated by TGA, and the thermograms are shown in Figure 3. The bare nanoparticles exhibit a small weight loss (∼2.5 wt %) below 300 °C due to the elimination of physically and chemically adsorbed water on their surface.[24] ESO exhibits a single degradation stage that initiates (T_i) at ∼300 °C and shows the maximum rate of weight loss (T_{max}) at ∼362 °C (see DTG curves in the inset of Figure 3), leading to the total decomposition of the material. This suggests that ESO produces only volatile compounds, consistent with previous studies[36] that identified the main thermal decomposition products of SO as short chain alkanes, aldehydes, and alcohols. A one-step process is also observed for the nanocomposites, due to the degradation of the cross-linked polymeric network, suggesting that the presence of ZnO hardly alters the degradation mechanism of the oil, and only the nanoparticles remain as residue. In fact, the residual mass of the

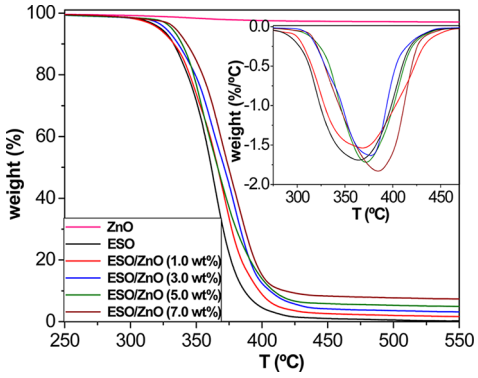

Figure 3. TGA curves under nitrogen atmosphere for ZnO, ESO, and the corresponding nanocomposites. The inset shows differential thermogravimetric analysis (DTG) curves of the polymeric samples.

nanocomposites (1.3, 2.9, 4.7 and 7.1%) approximately corresponds to their nanoparticle loading. A gradual rise in the degradation temperatures of the matrix is found with increasing ZnO content, by up to 20 and 17 °C in T_i and T_{max}, respectively, for the nanocomposite with 7.0 wt %. This thermal stability enhancement is related to the presence of homogeneously dispersed nanoparticles that act as a mass transport barrier and hinder the diffusion of volatile products generated during the decomposition process from the bulk of the composite to the gas phase. Other factors likely contributing to the thermal improvement are the high thermal conductivity of ZnO,[20] which should facilitate heat dissipation within the composite, as well as the strong nanofiller−matrix interactions that restrict thermal motion of the polymeric chains. An analogous behavior of thermal stability improvement has been reported for linseed oil nanocomposites reinforced with nanoclay[37] or polyhedral oligomeric silsesquioxane (POSS).[38]

Water Uptake and Barrier Properties. Biomaterials can be chemically damaged by long-term exposure to fluid environments; hence, low moisture absorption is desired in order to maintain their dimensional stability. The kinetics of water absorption of the nanocomposites was investigated, and the results are shown in Figure 4a.

All the samples exhibit a nonlinear growth of the water uptake with time, following Fick's law, reaching a constant value (equilibrium) after 2 weeks. ESO shows a low water uptake of ∼2.3% at equilibrium, consistent with its hydrophobic nature and high-cross-linking density. The addition of small amounts of ZnO reduces the water absorption, by ∼30% at 7.0 wt % loading. These results indicate that the nanocomposites have increased moisture resistance compared to the bioresin, which should be related to the presence of well-dispersed crystalline nanoparticles that increase the tortuosity of the transport path. Analogous behavior was described for epoxy composites reinforced with similar loadings of halloysite nanotubes (HNTs) or SiC nanoparticles.[39] The influence of ZnO concentration on the equilibrium water uptake is shown in the inset of Figure 4a. This property decreases gradually with increasing nanoparticle loading up to 5.0 wt %, while it remains almost unchanged at higher concentration. This behavior likely arises from a competition of water affinity and tortuosity effects. Although ZnO nanoparticles are more hydrophilic than ESO, consequently, the water affinity of the nanocomposites should increase with the nanoparticle content; the higher degree of tortuosity and the good nanoparticle dispersion outweigh this effect, and the overall result is a progressive drop in the water

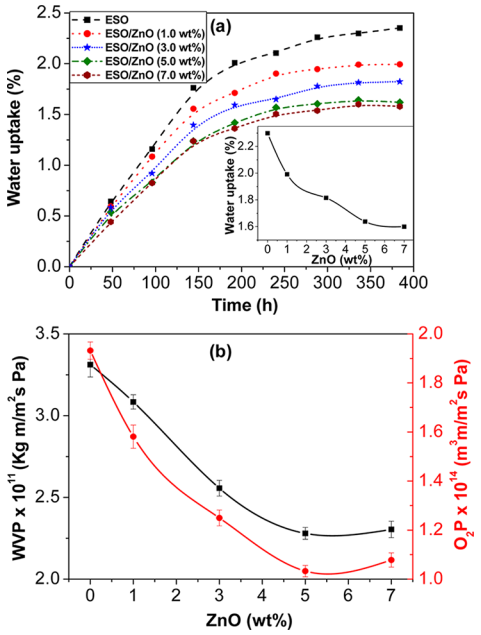

Figure 4. (a) Effect of ZnO on the water uptake of ESO thermoset. The inset displays the effect of ZnO loading on the equilibrium water uptake. (b) Water vapor permeability (WVP) and oxygen permeability (O_2P) as a function of nanoparticle content.

absorption. However, in the nanocomposite with the highest loading, the percentage of reduction in this property is similar to that of the sample with 5.0 wt % ZnO, likely due to the higher influence of the water affinity effect.

The WVP and O_2P were also investigated, and the data are plotted in Figure 4b. Neat ESO shows quite good water and oxygen permeability. As can be observed, both parameters drop gradually with increasing ZnO concentration, showing a minimum value (∼30 and 46% decrease, respectively) at a critical nanofiller loading of 5.0 wt %, which indicates enhanced barrier properties to gases for the nanocomposites in comparison to the biopolymer. This is consistent with SEM observations that revealed a lower degree of porosity for the composites and should be related to the very homogeneous ZnO dispersion and the increased tortuosity effect, as discussed above. However, raising the nanoparticle content to 7.0 wt % does not result in further gas permeability reduction, despite the increased ZnO−matrix interactions and the higher steric hindrance to the diffusion of gas molecules, probably due to the rise in the hydrophilicity of the system, which compensates for these effects. An analogous behavior has been reported for other biopolymer systems filled with ZnO,[24,35] where the gas permeability decreased significantly up to 5.0 wt % nanofiller loading and then remained merely unchanged. Overall, albeit the nanocomposites show improved barrier performance compared to the bioresin, their permeabilities are still high enough to ensure the transport of gases necessary for cell survival, which is important for their potential use as scaffolds.

Static Mechanical Properties. The appropriate mechanical performance for a biomaterial to be used in a tissue engineering application is critical to the success of the implant. The scaffold should have mechanical properties consistent with the anatomical site into which will be implanted, must be strong enough to allow surgical handling during implantation, and retain the mechanical strength until the completion of the remodeling process. A balance between mechanical properties

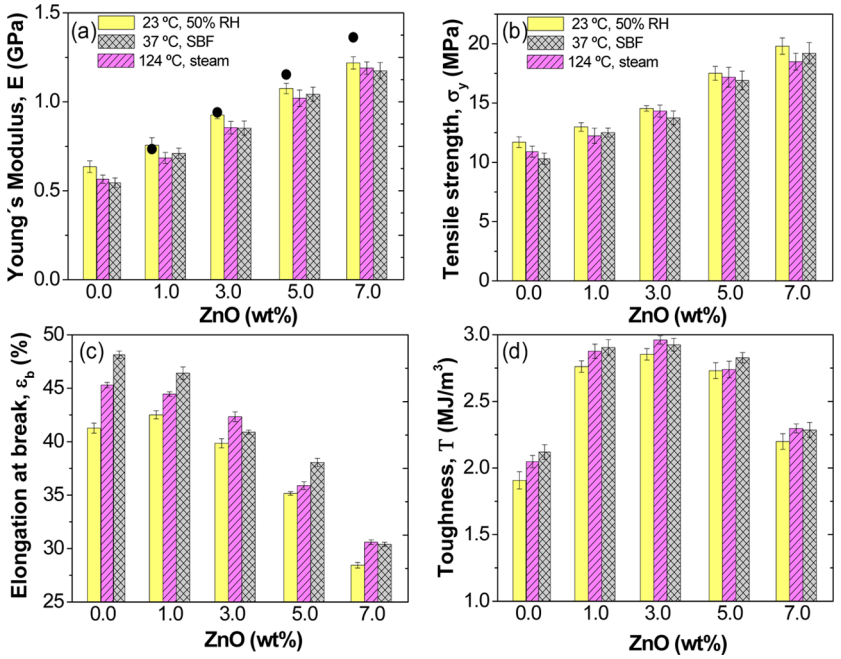

Figure 5. Comparison of the tensile properties of ESO/ZnO nanocomposites under different environmental conditions (see explanation in the text): (a) Young's modulus, (b) tensile strength, (c) elongation at break, and (d) toughness. The solid circles in part a correspond to the theoretical values according to the Krenchel's rule of mixtures.

and porous architecture is the key to the success of any scaffold. The static mechanical properties of ESO/ZnO nanocomposites were investigated by tensile tests, and their room temperature Young's modulus (E), tensile strength (σ_y), elongation at break (ε_b), and toughness (T) are compared in Figure 5. Cured ESO shows a E value of ~0.63 GPa (Figure 5a), comparable to that reported in the literature,[4] which increases gradually with nanoparticle loading, by up to 97% at the highest concentration. A very similar trend is found for σ_y, which exhibits a maximum improvement of ~46% at 7.0 wt % ZnO (Figure 5b). These exceptional improvements are ascribed to the reinforcement effect of the rigid and homogeneously dispersed nanoparticles that constraints polymer chain motion together with the strong nanofiller−matrix H-bonding interactions, a fact that promotes the adhesion between the two nanocomposite phases, resulting in improved load transfer. Taking into account the reported Young's modulus for ZnO,[20] the theoretical E values for ESO nanocomposites were calculated following Krenchel's rule of mixtures,[35] and the results are plotted as solid circles in Figure 5a. The predicted values are in good agreement with the experimental data (differences ≤10%). Since the model assumes individual nanoparticle dispersion and perfect nanofiller−matrix adhesion, the good correlation between theoretical and experimental values corroborates that the nanoparticles are indeed homogeneously dispersed and strongly adhered to the matrix.

With regard to ε_b (Figure 5c), ESO shows a high value (~42%) that remains merely unchanged at low ZnO loadings; this behavior is in contrast to that reported for traditional filler-reinforced composites, where higher rigidity is obtained at the expense of lowering the ductility. Similar or even higher ε_b values have also been reported upon addition of cellulose nanocrystals[40] or nanoclays[41] to castor oil, respectively. Nevertheless, a reduction in ε_b of ~31% is found for the highest nanofiller loading, likely related to the increased H-bonding interactions between the polar groups of ESO and the OH groups of ZnO that limit the ductile flow of the polymer chains. Another important parameter is the area under the tensile curve, which is a measure of the toughness of the system (Figure 5d). All the nanocomposites exhibit larger area than ESO, showing a maximum increment of ~50% at 3.0 wt % ZnO. These results indicate that the composites have enhanced ability to absorb energy during the deformation process.

Certain scaffolds are intended to remain in the body over a long period of time. Therefore, it is important to assess the mechanical properties of the nanocomposites under different conditions, such as long-term exposure to SBF at 37 °C, and to investigate if they can withstand several cycles in an autoclave, a method commonly used for medical implant sterilization. The results from tensile tests under those conditions are also shown in Figure 5. The comparison between data obtained before and after sterilization or exposure to SBF reveals that E and σ_y of all the samples decrease after being subjecting to aqueous conditions and high temperature compared to dry specimens, attributed to the plasticization effect of water absorption in ESO matrix. This can lead to a reduction in the ESO−ZnO interfacial strength and, hence, a drop in stiffness and strength. However, the drop in these parameters is stronger for the neat resin (21 and 17% in E and σ_y, respectively, under SBF conditions) compared to the nanocomposites (i.e., 7 and 11%, respectively, for the nanocomposite with 1.0 wt %), and the differences between dry and humid conditions decrease with increasing nanofiller loading, probably due to the reduction in water absorption, as discussed previously (Figure 4a). These results are consistent with those reported for HNT- or SiC-reinforced epoxy composites,[39] where the flexural strength and modulus decreased as a consequence of moisture absorption. Nevertheless, for similar nanofiller content, the falls found in those systems[39] are more pronounced than those observed in this work, likely related to the stronger ZnO−matrix interactions and, hence, improved stress transfer.

In contrast, ε_b and T increase due to exposure to a moist environment, ascribed to the enhanced flexibility of the samples owed to the plasticization effect of absorbed water and the more ductile flow of the polymer chains at high temperatures. In particular, for neat ESO, ε_b and T increase by 17 and 8%, respectively, under SBF conditions, whereas for the nanocomposites the changes are again smaller (i.e., ∼10 and 5% rise, respectively, at 1.0 wt % ZnO). Overall, despite the small reductions in stiffness and strength in physiological conditions compared to dry atmosphere, the nanocomposites display significantly improved performance than ESO, with enhancements by up to 130, 70, and 43% in E, σ_y, and T, respectively. Therefore, results demonstrate that these biomaterials are appropriate for long-term implant applications.

Thermomechanical Properties. The effect of ZnO nanoparticles on the dynamic mechanical properties of the composites was evaluated by DMA, and Figure 6 shows the temperature dependence of the storage modulus (E') and loss factor (tan δ) for ESO and the nanocomposites. The glass transition temperature (T_g) and E' values at different temperatures are collected in Table 2. E' of the composites rises gradually with the addition of ZnO both at temperatures below and above T_g, hinting toward the stiffening effect of these rigid nanoparticles and their good interaction with the matrix chains, as inferred from the FT-IR spectra. Thus, at −100 °C, the incorporation of 1.0, 3.0, 5.0, and 7.0 wt % nanoparticle content increases E' of ESO by ∼25, 33, 39, and 60%, respectively, whereas at temperatures above T_g the increments are even higher (i.e., ∼39, 87, 178, and 221% at 100 °C for the indicated loadings, Table 2), indicating that the stiffening effect is more pronounced above the softening point of the matrix. A similar trend has been reported for other ZnO-reinforced polymers, such as poly(ether ether ketone) (PEEK)[22] or poly(3-hydroxybutyrate-*co*-valerate) (PHBV).[24]

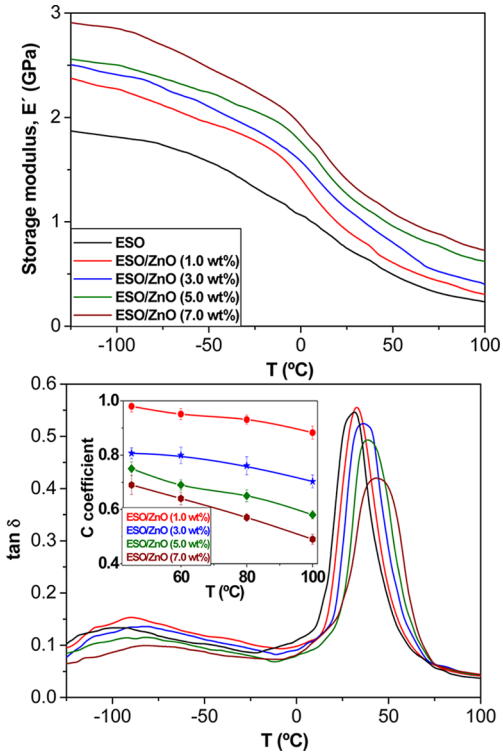

Figure 6. DMA data for ESO and the different nanocomposites: (top) storage modulus E' vs temperature and (bottom) tan δ as a function of temperature. The inset shows the C coefficient at the indicated temperatures.

The development of tan δ as a function of temperature reveals two relaxation peaks for all the samples. The transition at the lowest temperature (β-transition) is ascribed to the motion of aliphatic segments from the ring opening of the epoxide, while that at the highest temperature (α-transition or T_g) is attributed to Brownian motion of the main chains and the relaxation of associated dipoles.[42] β- And α-transitions appear at −96 and 31 °C for ESO. The incorporation of ZnO leads to an upshift of both transition temperatures, indicating restricted chain motion at the ESO−ZnO interface. In particular, T_g rises by ∼12 °C for the nanocomposite with 7.0 wt % loading compared to ESO (Table 2), ascribed to a very efficient barrier effect and decreased free volume. This increase is higher than that reported for an ESO nanocomposite with a similar amount of silica,[29] demonstrating the stronger barrier effect of ZnO nanoparticles.

A broadening of the tan δ peak is found upon addition of the nanoparticles, particularly for the nanocomposite with the highest loading (Table 2), which shows a full width at half-maximum (fwhm) ∼27% wider than that of ESO. This phenomenon is related to the difference between the physical state of the matrix surrounding the nanoparticles compared to the bulk matrix and has also been interpreted as a larger volume of the interface.[23] Moreover, the nanocomposites exhibit a reduced height of the tan δ peak compared to that of the neat thermoset (by up to 22% drop at 7.0 wt % ZnO, Table 2), another indication of the chain mobility constraint imposed by the nanoparticles. Further, the magnitude of tan δ is related to the degree of viscosity of a system: the higher the tan δ, the lower the elasticity of the material. Therefore, the lower tan δ in the nanocomposites suggests that when the stress is removed, the energy stored in deforming the material is recovered more quickly compared to the unfilled polymer.

The inset of Figure 6 shows the C coefficient values for the nanocomposites at different temperatures. This coefficient

Table 2. Thermomechanical Data for the Different Samples

material	T_g (°C)	$E'_{-100°C}$ (GPa)	$E'_{25°C}$ (GPa)	$E'_{100°C}$ (MPa)	tan δ_{max} (au)	fwhm (°C)	tan δ_{area} (au)	CTE (10^{-6}/°C) glassy	CTE (10^{-6}/°C) rubber	HDT (°C)
ESO	30.8	1.81	0.74	0.23	0.54	22.3	11.6	89.1	187.2	28.2
ESO/ZnO (1.0)	32.6	2.27	0.93	0.32	0.55	22.8	11.8	86.5	171.3	32.4
ESO/ZnO (3.0)	37.1	2.40	1.13	0.43	0.52	25.2	13.0	82.4	154.5	35.3
ESO/ZnO (5.0)	39.3	2.51	1.27	0.64	0.49	26.1	12.6	78.9	142.6	39.5
ESO/ZnO (7.0)	42.9	2.84	1.42	0.74	0.42	29.3	12.2	74.7	131.9	41.9

T_g, glass transition temperature; E', storage modulus; tan δ_{max}, peak height of tan δ; fwhm, full-width at half-maximum of tan δ peak; tan δ_{area}, area under tan δ peak; CTE, coefficient of thermal expansion; HDT, heat distortion temperature.

represents the ability to perturb the polymer chain motion; basically, the lower the coefficient, the higher the effectiveness of the reinforcement is. It can be calculated as $C = (E'_g/E'_r)_{comp}/(E'_g/E'_r)_{polym}$, where E'_g and E'_r are the storage modulus values in the glassy and rubbery region, respectively. For the calculations, four temperatures above T_g were selected (45, 60, 80, and 100 °C), taking E'_g at −50 °C. C drops with increasing nanoparticle loading, and the minimum values are obtained for the sample with 7.0 wt % ZnO. For all the nanocomposites, C decreases almost linearly with temperature, confirming the higher reinforcement effect at elevated temperatures; under such conditions, the E' of the polymer drops whereas that of the nanoparticles remains unchanged.

The effect of ZnO on the area under the tan δ peak was evaluated (Table 2), since this area is representative of the energy dissipated in the viscoelastic relaxations and can be correlated with the impact strength of the material (Figure 7).

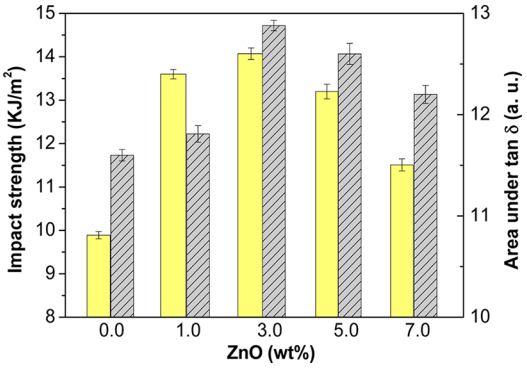

Figure 7. Comparison of the Charpy notched impact strength (solid bars) and the area under tan δ curve (dashed bars) for cured ESO and its nanocomposites.

In fact, any molecular process that promotes energy dissipation improves the impact resistance of the sample.[43] All the nanocomposites exhibit larger area than ESO, showing a maximum increase of ∼12% at 3.0 wt % ZnO. A similar trend is found for the Charpy impact strength, which rises upon addition of the nanoparticles, and the highest improvement (∼58%) is also attained at 3.0 wt % loading. This dependence of the impact strength on the nanoparticle concentration was already anticipated from the area under the tensile curves, and the results from the three techniques display a very similar tendency. Overall, data demonstrate that the incorporation of these nanoparticles simultaneously improves the matrix stiffness and its ability to dissipate energy, and the optimal ZnO concentration ranges from 3.0 to 7.0 wt %.

The heat distortion temperature is an important parameter for product design, particularly for load-bearing applications at temperatures above ambient. Several factors influence the HDT of polymeric materials, including the stiffness and the T_g.[44] The addition of increasing ZnO contents to ESO leads to a gradual raise in this parameter (Table 2), by up to 13 °C (49% rise) at 7.0 wt % loading. These noteworthy improvements arise from the simultaneous increase in rigidity and T_g in the nanocomposites. This behavior is in contrast to that reported upon incorporation of organoclay to diglycidyl ether of bisphenol A (DGEBA)/ESO blends,[45] where the plasticizing effect of the clay decreased both the HDT and T_g.

Another thermomechanical property used in the design of materials for implant applications is the coefficient of thermal expansion. A low CTE is required to maintain the material dimensional stability, and it can be obtained by dispersing low CTE particles like ZnO.[21] Table 2 collects CTE data in the glassy and rubbery states. In both cases, the CTE of the resin drops progressively with increasing ZnO loading, since the homogeneously dispersed nanoparticles restrict its thermally

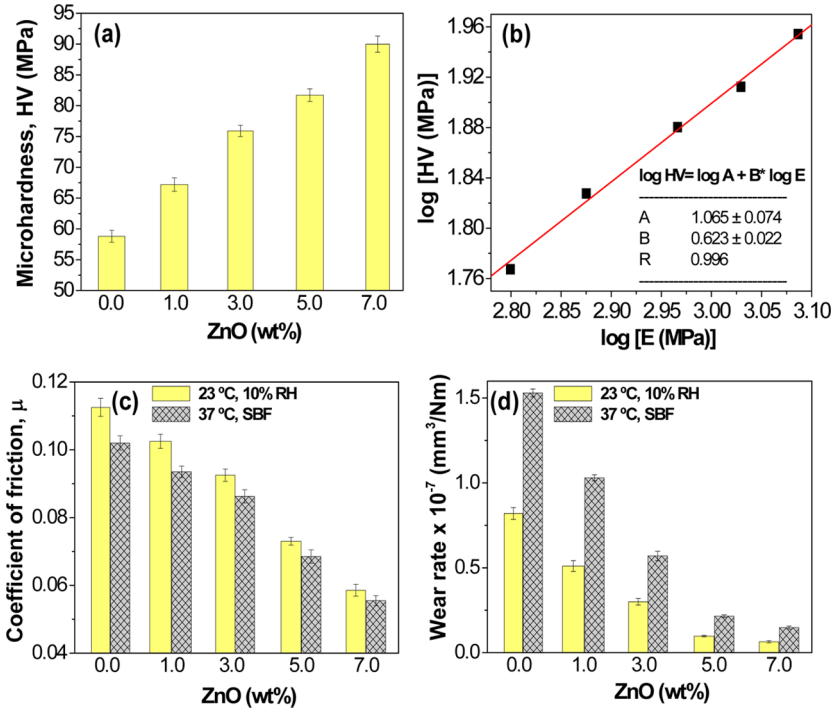

Figure 8. (a) Vickers microhardness (HV) data for ESO and the nanocomposites with different ZnO loading, (b) linear relationship between microhardness and Young's modulus (log–log scale), (c) coefficient of friction, and (d) wear rate under dry and SBF conditions.

induced movements. This reduction also arises from the characteristics of the nanoparticles (low CTE, high modulus, spherical shape). The CTE reduction in the rubbery region is systematically stronger than in the glassy state. For instance, at 7.0 wt % loading, the drop at $T > T_g$ is ~27%, about double that observed in the glassy state, consistent with the stronger reinforcement effect found at high temperatures by DMA (Figure 6). Analogous behavior was found upon addition of other spherical inorganic nanoparticles such as IF-WS_2 to poly(phenylene sulfide) (PPS),[46] explained in terms of the higher differences in stiffness and thermal expansion between the polymer and the nanofiller at $T > T_g$.

Microhardness and Tribological Properties. From an application viewpoint, particularly for implant uses, it is important to assess the hardness and tribological performance of these nanocomposites. Their Vickers microhardness (HV) data are compared in Figure 8a. The HV of ESO is ~58 MPa and increases linearly with the ZnO content, the increment being ~55% at 7.0 wt % loading. The homogeneous nanoparticle dispersion combined with the reduction in the interparticle distance with increasing ZnO concentration led to an improvement in the resistance to local plastic deformation and, hence, a rise in microhardness. A direct relationship is frequently found between the Young's modulus obtained from tensile tests and the Vickers microhardness:[47] $HV = aE^b$, where a and b are constants. This equation is fulfilled in many polymeric systems including bioglass/high-density polyethylene composites for soft tissue applications.[48] ESO/ZnO nanocomposites show a very good linear relationship when plotting log HV vs log E, as depicted in Figure 8b.

The tribological performance of biomaterials is one of the main aspects of implant surgery. Wear particles are formed in a piece of bone or cartilage if it rubs against the implant or if two parts of the implant rub against each other. The presence of these wear products in the tissue surrounding the implant might lead to periprosthetic bone loss and, hence, undesirable tissue reactions like inflammation, which can provoke loosening due to osteolysis.[49] In this regard, the triglyceride structure of vegetable oils can generate lubricant films that interact strongly with metallic surfaces, reducing both friction and wear.[50] The coefficient of friction (μ) and the specific wear rate (W_{sp}) of the nanocomposites were evaluated under both dry atmosphere at 23 °C and SBF environment at 37 °C, and the results are plotted in parts c and d of Figure 8, respectively. Under dry condition, μ of ESO is ~0.11, and it falls gradually with increasing ZnO content, by up 51% at the highest loading. This behavior can be attributed to several factors, including the improvement in mechanical properties (i.e., modulus, strength, hardness), the presence of uniformly dispersed hard nanoparticles that can restrain the scuffing and adhesion of the resin during sliding, and the increase in thermal conductivity that lowers the temperature in the sliding contact. A very similar trend is found in SBF, where μ falls from ~0.1 for neat ESO to ~0.056 for the nanocomposite with 7.0 wt % loading; in this case, the decrease in μ of the resin is smaller compared to that under dry conditions, in agreement with the fact that the nanoparticles exert lower reinforcing effect under SBF environment, as revealed by tensile tests. The μ values are systematically lower in SBF, since the aqueous medium lubricates the surfaces in contact and can absorb most of the frictional heat. This is consistent with previous studies[50] on the tribological behavior of vegetable oils that reported a decrease in μ with increasing humidity, ascribed to the reaction of the fatty acid chains with the metallic countersurface via oxide film formation, producing multilayers of soap, a process that was favored in the presence of water. Other factors, like the interaction of the polymer with water and the surface wettability, can also play an important role on the friction and wear of the nanocomposites under aqueous conditions. Further, the differences between μ values obtained under dry and aqueous environments decrease with increasing ZnO loading, likely related to the reduction in water absorption.

Regarding the wear rate (Figure 8d), a very strong drop is found upon incorporation of the nanoparticles to ESO under both environments. In particular, the nanocomposite with the highest loading shows ~12- and 10-fold decrease in W_{sp} under dry and SBF conditions, respectively. This behavior is likely related to the superior mechanical properties of this nanocomposite, its homogeneous nanoparticle dispersion, and strong ESO−ZnO interfacial adhesion via H-bonding interactions, facts that result in the development of a thin and uniform transfer film and, hence, better tribological properties.[23] It has been proposed that spherical inorganic nanoparticles like TiO_2[51] or IF-WS_2[52] embedded in an epoxy matrix can act as ball-bearing components and roll rather than slide between the composite surface and its counterpart. Such a rolling mechanism could explain the reductions in μ and W_{sp} observed in this work. It can also be observed from Figure 8d that W_{sp} in SBF is systematically higher (on average double) than in the dry state, consistent with previous studies[50] that compared the wear of vegetable oils under different humidity conditions. The plasticization of the thermoset surface could contribute to the increase in wear rate in SBF. If water diffused through ESO and the nanocomposites, swelling could lead to a reduction in the degree of chain cross-linking and, hence, a drop in hardness and strength that enabled the polymer fibrils to be detached more easily, thereby decreasing the wear resistance. Further, the differences between data for dry and aqueous conditions become smaller with increasing nanoparticle loading, related to the decrease in the water absorption (Figure 4), hence corroborating the influence of the plasticization effect. Another potential explanation for the behavior observed is that in SBF the hydraulic action disrupted the formation of the transfer layer and promoted direct contact between the film and counterface, leading to an increased wear rate. Besides, the SFB can contain wear debris that have an abrasive effect on the material. Overall, results demonstrate considerably improved tribological performance for the nanocomposites compared to the neat thermoset, which is interesting with a view to use them for tissue engineering applications.

Antibacterial Activity. The antibacterial activity of ESO nanocomposites was evaluated with and without UV irradiation against two bacteria, *E. coli* (Gram-negative) and *S. aureus* (Gram-positive), and the results are plotted in Figure 9. *S. aureus* is one of the most common causes of postoperative infection; hence, it is interesting to investigate the bactericidal effects against this microorganism from a clinical viewpoint. The ISO 22196:2007 stipulates that efficient antibacterial activity should be higher than 2. Neat ESO exhibits some antimicrobial effect, ~0.1 and 0.4 against *E. coli* and *S. aureus*, respectively, under both irradiated and nonirradiated conditions. This behavior is in agreement with recent reports regarding bactericidal activity of vegetable oils that found a more effective action against Gram-positive bacteria.[53] Besides, previous studies reported that fatty acids can hinder the growth

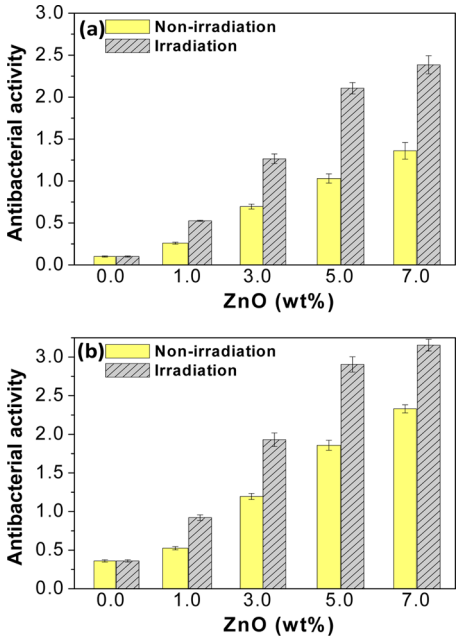

Figure 9. Antibacterial activity of ESO/ZnO nanocomposites against (a) *E. coli* and (b) *S. aureus*. Solid and dashed bars correspond to experiments performed without and with UV irradiation, respectively.

of many bacteria,[54] and their antimicrobial activity was dependent on the chain length and unsaturation degree: the longer the chain, the higher the inhibition was. Figure 9 reveals that the antibacterial action improves on increasing nanoparticle content both in the presence and the absence of UV light. This trend is a consequence of the homogeneous nanoparticle distribution in the composites. In fact, for uniformly dispersed fillers, the higher the concentration, the larger the effective surface area for interaction with the bacteria is. Under UV illumination, *E. coli* activity was inhibited when ZnO concentration was ≥5.0 wt %, while *S. aureus* growth was suppressed by all the composites except for that with the lowest loading (1.0 wt %). This is consistent with previous studies on ZnO-reinforced polyurethane[53,55] that found a more effective antibacterial activity against Gram-positive bacteria. The production of H_2O_2 is the main mechanism responsible for the antibacterial activity of ZnO, and this photocatalysis process has been described by Hoffmann et al.[56] and is related to the generation of reactive oxygen species (ROS), including O_2^-, HO_2, and HO radicals. This strong oxidizing power typically results in the lysis of microorganisms. The different behavior against the two types of bacteria is most likely related to structural and chemical compositional differences of the cell surfaces.[57,58] The denser and more complex cell structure of *E. coli* should lessen the damage from oxidation radicals.

Experimental results show that these bionanocomposites possess antibacterial activity, even in the absence of photoirradiation, in agreement with studies that explored the antibacterial activity of ZnO without illumination.[25,59] Under such conditions, ESO/ZnO nanocomposites are only moderately toxic to *E. coli* (∼1.4 antibacterial activity at the highest nanoparticle loading, Figure 9a), while ZnO concentrations ≥5.0 wt % lead to remarkable toxic effect on *S. aureus*, as depicted in Figure 9b. Despite the generation of ROS as the primary reason for ZnO toxicity in the presence of UV light,[54] the foremost cause of cytotoxicity without irradiation remains unclear, and several mechanisms have been proposed:[25,60] the release of Zn^{2+}, the internalization of the nanoparticles in the cell and destruction of the bacteria from the interior, and the nanoparticle adsorption on the cell surface causing ZnO−cell physicochemical interactions that cause cellular damage. Further, few authors[25,59] have given evidence for H_2O_2 formation in the absence of light. The process seems to be related with the moisture absorption,[61] albeit the mechanism is not clear. Our results demonstrate the great potential of these nanocomposites to induce an antibacterial property, which is interesting for biomedical applications.

4. CONCLUSIONS

In this study, different ZnO loadings were incorporated into an epoxidized soybean oil via simple ultrasonication and curing. The morphology, water absorption, thermal, mechanical, tribological, barrier, and antibacterial properties of the resulting bionanocomposites were analyzed. FT-IR spectra corroborated the existence of strong H-bonding interactions between the hydroxyl moieties of ZnO and the polar groups of the bioresin. SEM images revealed a random and uniform nanoparticle dispersion within the ESO matrix. TGA experiments showed a strong rise in thermal stability upon increasing ZnO concentration. The nanoparticles reduced the water uptake and water and oxygen permeability due to the increased tortuosity of the transport pathways. Remarkable improvements in the storage modulus, glass transition temperature, Young's modulus, tensile strength, toughness, hardness, and heat distortion temperature were attained, demonstrating the strong reinforcing effect of these nanoparticles. The stiffness and strength of the nanocomposites slightly decreased after exposure to several cycles of steam sterilization in an autoclave or to SBF at 37 °C, albeit they were well above the values obtained for the neat thermoset. The CTE was steadily reduced with increasing ZnO content both in the glassy and rubbery state, since the nanoparticles hinder the thermally induced movements of the polymeric chains. Exceptional enhancements in the tribological performance under both dry and SBF conditions were achieved, corroborating the suitability of these nanoparticles for improving the wear resistance of the bioresin. Under or without UV irradiation, the nanocomposites exhibited antimicrobial activity against both Gram-negative and Gram-positive bacteria, and the effectiveness increased with the nanoparticle concentration. The antibacterial action toward *S. aureus* was stronger than that toward *E. coli*. These novel biodegradable and biocompatible nanocomposites show an optimal combination of mechanical, thermal, fluid transport, and antibacterial properties; are inexpensive and environmentally friendly; and their manufacturing process is simple and very easy to scale up, hence making these nanocomposites very promising for biomedical uses, particularly as porous scaffolds for soft tissue applications.

AUTHOR INFORMATION

Corresponding Author

*E-mail: am.diez@uah.es.

Notes

The authors declare no competing financial interest.

ACKNOWLEDGMENTS

Dr. Ana Diez-Pascual wishes to acknowledge the Ministerio de Economía y Competitividad (MINECO) for a "Ramón y Cajal" Senior Research Fellowship cofinanced by the EU.

REFERENCES

(1) Raqueza, J.-M.; Deléglisea, M.; Lacrampea, M.-F.; Krawczaka, P. Thermosetting (Bio)materials Derived from Renewable Resources: A Critical Review. *Prog. Polym. Sci.* **2010**, *35*, 487−509.

(2) Gunstone, F. *Fatty Acid & Lipid Chemistry*; Blackie Academic & Professional: New York, 1996; pp 1−252.

(3) Allen, R. R.; Formo, M. V.; Krishnamurthy, R. G.; McDermott, G. N.; Norris, F. A.; Sonntag, N. O. V. *Bailey's Industrial Oil and Fat Products*. Wiley: New York, 1982.

(4) Mosiewicki, M. A.; Aranguren, M. I. A Short Review on Novel Biocomposites Based on Plant Oil Precursors. *Eur. Polym. J.* **2013**, *49*, 1243−1256.

(5) Meier, M. A. R.; Metzger, J. O.; Schubert, U. S. Plant Oil Renewable Resources as Green Alternatives in Polymer Science. *Chem. Soc. Rev.* **2007**, *36*, 1788−1802.

(6) Lu, Y.; Larock, R. C. Novel Biobased Nanocomposites from Soybean Oil and Functionalized Organoclay. *Biomacromolecules* **2006**, *7*, 2692−2700.

(7) Zhu, L.; Wool, R. P. Nanoclay Reinforced Bio-Based Elastomers: Synthesis and Characterization. *Polymer* **2006**, *47*, 8106−8115.

(8) Kiatsimkul, P.-P.; Suppes, G. J.; Hsieh, F.-H.; Lozada, Z.; Tu, Y.-C. Preparation of High Hydroxyl Equivalent Weight Polyols from Vegetable Oils. *Ind. Crops. Prod.* **2008**, *27*, 257−264.

(9) Seniha-Güner, F.; Yagci, Y.; Tuncer-Erciyes, A. Polymers from Triglyceride Oils. *Prog. Polym. Sci.* **2006**, *31*, 633−670.

(10) Liu, Z.; Erhan, S. Z. Ring-Opening Polymerization of Epoxidized Soybean Oil. *J. Am. Oil. Chem. Soc.* **2010**, *87*, 437−444.

(11) Burt, S. A. Essential Oils: Their Antibacterial Properties and Potential Applications in Foods—A Review. *Int. J. Food Microbiol.* **2004**, *94*, 223−253.

(12) Santin, M.; Ambrosio, L. Soybean-Based Biomaterials: Preparation, Properties and Tissue Regeneration Potential. *Expert Rev. Med. Devices* **2008**, *5*, 349−358.

(13) Wong, H. L.; Rauth, A. M.; Bendayan, R.; Manias, J. L.; Ramaswamy, M.; Liu, Z. S.; Erhan, S. Z.; Wu, X. Y. A New Polymer−Lipid Hybrid Nanoparticle System Increase Cytotoxicity of Doxorubicin against Multidrug-Resistant Human Breast Cancer Cells. *Pharm. Res.* **2006**, *23*, 1574−1585.

(14) Miao, S.; Sun, L.; Wang, P.; Liu, R.; Su, Z.; Zhang, S. Soybean Oil-Based Polyurethane Networks as Candidate Biomaterials: Synthesis and Biocompatibility. *Eur. J. Lipid Sci. Technol.* **2012**, *114*, 1165−1174.

(15) Ulery, B. D.; Nair, L. S.; Laurencin, C. T. Biomedical Applications of Biodegradable Polymers. *J. Polym. Sci., Part B: Polym. Phys.* **2011**, *49*, 832−864.

(16) Miao; Wang, P.; Su, Z.; Zhang, S. Vegetable-Oil-Based Polymers as Future Polymeric Biomaterials. *Acta Biomater.* **2014**, *10*, 1692−1704.

(17) Wool, R. P. Polymers and Composite Resins from Plant Oils. In *Bio-Based Polymers and Composites*; Sun, X. S., Ed.; Elsevier: Burlington, VT, 2005.

(18) Goud, V. V.; Patwardhan, A. V.; Pradhan, N. C. Epoxidation of Karanja (*Pongamia glabra*) Oil by H_2O_2. *J. Am. Oil Chem. Soc.* **2006**, *83*, 635−640.

(19) Guenter, S.; Rieth, R.; Rowbottom, K. T. Epoxides. In *Ullmann's Encyclopaedia of Industrial Chemistry*, 6th ed., Pelc, H., Ed.; John Wiley & Sons Ltd: Chichester, UK 2003; Vol. *12*; pp 269−284.

(20) Coleman, A.; Jagadish, C. Basic Properties and Applications of ZnO. In *Zinc Oxide Bulk, Thin Films and Nanostructures*; Jagadish, C., Pearton, S., Eds.; Elsevier: Burlington, VT, 2006.

(21) Adachi, S. *Properties of Group-IV, III-V and II-VI Semiconductors*; John Wiley & Sons Ltd: Chichester, UK, 2005.

(22) Diez-Pascual, A. M.; Xu, C. P.; Luque, R. Development and Characterization of Novel Poly(ether ether ketone)/ZnO Bionanocomposites. *J. Mater. Chem. B* **2014**, *2*, 3065−3078.

(23) Diez-Pascual, A. M.; Diez-Vicente, A. L. High-Performance Aminated Poly(phenylene sulfide)/ZnO Nanocomposites for Medical Applications. *ACS Appl. Mater. Interfaces* **2014**, *6*, 10132−10145.

(24) Diez-Pascual, A. M.; Diez-Vicente, A. L. ZnO-Reinforced Poly(3-hydroxybutyrate-*co*-3-hydroxyvalerate) Bionanocomposites with Antimicrobial Function for Food Packaging. *ACS Appl. Mater. Interfaces* **2014**, *6*, 9822−9834.

(25) Yamamoto, O. Influence of Particle Size on the Antibacterial Activity of Zinc Oxide. *Int. J. Inorg. Mater.* **2001**, *3*, 643−646.

(26) Sawai, J. Quantitative Evaluation of Antibacterial Activities of Metallic Oxide Powders (ZnO, MgO and CaO) by Conductimetric Assay. *J. Microbiol. Methods* **2003**, *54*, 177−182.

(27) Khot, S. N.; La Scala, J. J.; Can, E.; Morye, S. S.; Williams, G. I.; Palmese, G. R.; Kusefoglu, S. H.; Wool, R. P. Development and Application of Triglyceride-Based Polymers and Composites. *J. Appl. Polym. Sci.* **2001**, *82*, 703−723.

(28) Liu, Z.; Erhan, S. Z.; Akin, D. E.; Barton, F. E. "Green" Composites from Renewable Resources: Preparation of Epoxidized Soybean Oil and Flax Fiber Composites. *J. Agric. Food Chem.* **2006**, *54*, 2134−2137.

(29) Zhan, G.; Tang, X.; Yu, Y.; Li, S. Biobased Cyanate Ester Composites with Epoxidized Soybean Oil and in Situ Generated Nano-Silica. *Polym. Eng. Sci.* **2011**, *51*, 426−433.

(30) Zhang, J.; Hu, S.; Zhan, G.; Tang, X.; Yu, Y. Biobased Nanocomposites from Clay Modified Blend of Epoxidized Soybean Oil and Cyanate Ester Resin. *Prog. Org. Coat.* **2013**, *76*, 1683−1690.

(31) Dinda, S.; Patwardhan, A. V.; Goud, V. V.; Pradhan, N. C. Epoxidation of Cottonseed Oil by Aqueous Hydrogen Peroxide Catalysed by Liquid Inorganic Acids. *Bioresour. Technol.* **2008**, *99*, 3737−3744.

(32) Hanks, J. H.; Wallace, R. E. Relation of Oxygen and Temperature in the Preservation of Tissues by Refrigeration. *Proc. Soc. Exp. Biol. Med.* **1949**, *71*, 196−200.

(33) Sinclair, R. G.; McKay, A. F.; Jones, R. N. The Infrared Absorption Spectra of Saturated Fatty Acid and Esters. *J. Am. Chem. Soc.* **1952**, *74*, 2570−2575.

(34) Colthup, N. B.; Day, L. H.; Wiberley, S. E. *Introduction to Infrared and Raman Spectroscopy*, 3rd ed.; Academic Press, Inc.: San Diego, CA, 1990.

(35) Diez-Pascual, A. M.; Diez-Vicente, A. L. Poly(3-hydroxybutyrate)/ZnO Bionanocomposites with Improved Mechanical, Barrier and Antibacterial Properties. *Int. J. Mol. Sci.* **2014**, *15*, 10950−10973.

(36) Mahungu, S. M.; Hansen, S. L.; Artz, W. E. Volatile Compounds in Heated Oleic Acid-Esterified Propoxylated Glycerol. *J. Am. Oil Chem. Soc.* **1998**, *75*, 683−690.

(37) Sharma, V.; Banait, J. S.; Larock, R. C.; Kundu, P. P. Synthesis and Characterization of Linseed Oil-Based Nanocomposites. *Polym. Compos.* **2010**, *31*, 630−637.

(38) Lligadas, G.; Ronda, J. C.; Galia, M.; Cadiz, V. Bionanocomposites from Renowable Resources: Epoxidized Linseed Oil-Polyhedral Oligomeric Silsesquioxanes Hybrid Materials. *Biomacromolecules* **2006**, *7*, 3521−3526.

(39) Alamri, H.; Low, I. M. Effect of Water Absorption on the Mechanical Properties of Nano-Filler Reinforced Epoxy Nanocomposites. *Mater. Des.* **2012**, *42*, 214−222.

(40) Gao, Z.; Peng, J.; Zhong, T.; Sun, J.; Wang, X.; Yue, C. Biocompatible Elastomer of Waterborne Polyurethane based on Castor Oil and Polyethylene Glycol with Cellulose Nanocrystals. *Carbohydr. Polym.* **2012**, *87*, 2068−2075.

(41) Kaushik, A.; Ahuja, D.; Salwani, V. Synthesis and Characterization of Organically Modified Clay/Castor Oil Based Chain Extended Polyurethane Nanocomposites. *Composites Part A* **2011**, *42*, 1534−1541.

(42) Gonzalez-Dominguez, J. M.; Anson-Casaos, A.; Diez-Pascual, A. M.; Ashrafi, B.; Naffakh, M.; Backman, D.; Stadler, H.; Johnston, A.; Gomez, M.; Martinez, M. T. Solvent-Free Preparation of High-Toughness Epoxy−SWNT Composite Materials. *ACS Appl. Mater. Interfaces* **2011**, *3*, 1441−1450.

(43) Diez-Pascual, A. M.; Naffakh, M.; González-Domínguez, J. M.; Ansón, A.; Martínez-Rubi, Y.; Martínez, M. T.; Simard, B.; Gomez, M. A. High Performance PEEK/Carbon Nanotube Composites Compati-

bilized with Polysulfones-II. Mechanical and Electrical Properties. *Carbon* **2010**, *48*, 3500−3511.
(44) Diez-Pascual, A. M.; Naffakh, M. Enhancing the Thermomechanical Behaviour of Poly(phenylene sulphide) Based Composites via Incorporation of Covalently Grafted Carbon Nanotubes. *Composites Part A* **2013**, *54*, 10−19.
(45) Sithique, M. A.; Alagar, M. Preparation and Properties of Bio-Based Nanocomposites From Epoxidized Soy Bean Oil and Layered Silicate. *Malaysian Polym. J.* **2010**, *5*, 151−161.
(46) Diez-Pascual, A. M.; Naffakh, M. Inorganic Nanoparticle-Modified Carbon Fiber Fabric/Poly(phenylene sulphide) Laminates with Enhanced Thermomechanical Behaviour. *Materials* **2013**, *6*, 3171−3193.
(47) Baltá Calleja, F. J. Microhardness Relating to Crystalline Polymers. *Adv. Polym. Sci.* **1985**, *66*, 117−148.
(48) Wang, M.; Hench, L. L.; Bonfield, W. Bioglass/High Density Polyethylene Composite for Soft Tissue Applications: Preparation and Evaluation. *J. Biomed. Mater. Res.* **1998**, *42*, 577−586.
(49) Williams, D. F. The Deterioration of Materials Used as Implants in Surgery. In *Implants in Surgery*; Williams, D. F., Roaf, R., Maisels, D. O., Eds.; W. B. Saunders Co.: Philadelphia, PA, 1973; p 173.
(50) Siniawski, M. T.; Saniei, N.; Stoyanov, P. Influence of Humidity on the Tribological Performance of Unmodified Soybean and Sunflower Oils. *Lubr. Sci.* **2011**, *23*, 301−311.
(51) Chang, L.; Zhang, Z. Tribological Properties of Epoxy Nanocomposites: II. A Combinative Effect of Short Carbon Fiber and Nano-TiO_2. *Wear* **2006**, *260*, 869−878.
(52) Rapoport, L.; Nepomnyashcy, O.; Verdyan, A.; Popovitz-Biro, R.; Volovik, Y.; Ittah, B.; Tenne, R. Polymer Nanocomposites with Fullerene-like Solid Lubricant. *Adv. Eng. Mater.* **2004**, *6*, 44−48.
(53) Yari, A.; Yeganeh, H.; Bakhshi, H.; Gharibi, R. Preparation and Characterization of Novel Antibacterial Castor Oil-Based Polyurethane Membranes for Wound Dressing Application. *J. Biomed. Mater. Res. Part A* **2014**, *102A*, 84−96.
(54) Knapp, H. R.; Melly, M. A. Bactericidal Effects of Polyunsaturated Fatty Acids. *J. Infect. Dis.* **1986**, *154*, 84−94.
(55) Zvekić, D.; Srdić, V. V.; Karaman, M. A.; Matavulj, M. N. Antimicrobial Properties of ZnO Nanoparticles Incorporated in Polyurethane Varnish. *Process. Appl. Ceram.* **2011**, *5*, 41−45.
(56) Hoffmann, M. R.; Martin, S. T.; Choi, W. Y.; Bahnemann, D. W. Environmental Applications of Semiconductor Photocatalysis. *Chem. Rev.* **1995**, *95*, 69−96.
(57) Cabeen, M. T.; Jacobs-Wagner, C. Bacterial Cell Shape. *Nat. Rev. Microbiol.* **2005**, *3*, 601−610.
(58) Diez-Pascual, A. M.; Diez-Vicente, A. L. Development of Nanocomposites Reinforced with Carboxylated Poly(ether ether ketone)-Grafted to Zinc Oxide with Superior Antibacterial Properties. *ACS Appl. Mater. Interfaces* **2014**, *6*, 3729−3741.
(59) Tam, K. H.; Djurišić, A. B.; Chan, C. M. N.; Xi, Y. Y.; Tse, C. W.; Leung, Y. H.; Chan, W. K.; Leung, F. C. C.; Au, D. W. T. Antibacterial Activity of ZnO Nanorods Prepared by a Hydrothermal Method. *Thin Solid Films* **2008**, *516*, 6167−6174.
(60) Brayner, R.; Ferrari-Iliou, R.; Brivois, N.; Djediat, S.; Benedetti, M. F.; Fievet, F. Toxicological Impact Studies Based on *Escherichia coli* Bacteria in Ultrafine ZnO Nanoparticles Colloidal Medium. *Nano Lett.* **2006**, *6*, 866−870.
(61) Ghule, K.; Ghule, A. V.; Chen, B.-J.; Ling, Y.-C. Preparation and Characterization of ZnO Nanoparticles Coated Paper and Its Antibacterial Activity Study. *Green Chem.* **2006**, *8*, 1034−1041.